# Fabrication of Diverse Metallic Nanowire Arrays Based on Block Copolymer Self-Assembly

**ARTICLE** *in* NANO LETTERS · SEPTEMBER 2010

Impact Factor: 13.59 · DOI: 10.1021/nl1023518 · Source: PubMed

NANO LETTERS

pubs.acs.org/NanoLett

# Fabrication of Diverse Metallic Nanowire Arrays Based on Block Copolymer Self-Assembly

**Yeon Sik Jung,[†,‡] Ju Ho Lee,[‡] Jeong Yong Lee,[‡] and C. A. Ross*[,†]**

[†]Department of Materials Science and Engineering, Massachusetts Institute of Technology, 77 Massachusetts Avenue, Cambridge, Massachusetts 02139 and [‡]Department of Materials Science and Engineering, Korea Advanced Instute of Science and Technology (KAIST), 335 Gwahak-ro, Yuseong-gu, Daejeon 305-701, Republic of Korea

**ABSTRACT** Metallic nanowires are useful for fabricating highly integrated nanoscale electrical, magnetic, and photonic devices. However, conventional methods based on bottom-up growth techniques are subject to concerns such as broad distributions in their dimension as well and difficulties in precise placement of the nanowires. These issues can be solved by the guided self-assembly of block copolymer thin films that can produce periodic arrays of monodisperse nanoscale features with excellent positional accuracy. Here, we report transfer of high-quality linear block copolymer patterns into various metals, Ti, W, Pt, Co, Ni, Ta, Au, and Al, to fabricate highly ordered nanowire arrays with widths down to 9 nm. This novel patterning process does not require specific film deposition techniques or etch-chemistries. We also describe their structural, magnetic, and electrical properties.

**KEYWORDS** Block copolymer lithography, metallic nanowires, magnetic nanowires, metal gratings, polystyrene–polydimethylsiloxane

For the past decade, there has been enormous interest in inorganic one-dimensional nanostructures,[1,2] and due to their unprecedented properties in the sub-100-nm regime, various kinds of electric, optical, optoelectronic, and biological devices based on nanowires or nanotubes have been demonstrated.[1−4] Nanowires are often fabricated directly by vapor deposition processes such as the vapor–liquid–solid technique, in which the dimensions, composition, and crystallographic orientation can be controlled by manipulating various synthetic parameters.[5] However, these methods are frequently accompanied by inherent issues such as broad distributions in the length and properties of synthesized nanowires, limitations on available compositions, and difficulties in placing the nanowires precisely onto a substrate. To position the nanowires into specific locations on substrates requires additional methods based on, for example, electric or fluidic fluids.[6,7] Alternatively, techniques based on planar processing can be used to fabricate nanowires directly on a substrate such that their composition, dimensions, position, and orientation can easily be controlled. However, these methods are limited by the resolution of the lithography system used to make them, and in the case of electron-beam lithography, the low throughput. It is therefore valuable to develop alternative methods for nanowire fabrication which can rapidly produce nanowires of arbitrary composition and narrow line width.

Block copolymer (BCP) nanolithography is well suited for fabrication of nanoscale structures due to its fine resolution, cost-effectiveness, and scalability. BCPs consist of two or more incompatible polymer blocks that form a single polymeric chain and can undergo microphase separation to form periodic nanostructures.[8] The morphology and length scale of the self-assembled patterns usually range from ∼10 to 100 nm and can be controlled by the degree of polymerization and the volume fraction of the blocks. Selective removal of one block leaves a pattern that can be used as a mask for fabricating functional nanostructures such as magnetic particles,[9] phase-changing chalcogenide dots,[10] or silicon nanowires[11] via reactive ion etching, ion-milling, or lift-off processes. BCPs have also been used to template certain metallic nanowires by selective incorporation of metallic elements into a polypyridine block followed by elimination of organic components using an oxygen plasma treatment.[4]

We previously reported that poly(styrene-*b*-dimethylsiloxane) (PS-PDMS) diblock copolymers with a large Flory–Huggins interaction parameter can generate sub-15-nm wide patterns of 32–40 nm period with excellent long-range ordering and reliability.[12−15] Our prior work also showed that oxidized PDMS patterns obtained from the BCP can be used as a robust etch mask to pattern soft polymeric films such as a conducting polymer using an oxygen etch[15] and for patterning metal films into dot, ring, line, and antidot arrays.[16,17] (Figures S1 and S2 in the Supporting Information show another example of pattern transfer into a polymer resin.) In this Letter, we demonstrate transfer of high-quality linear patterns into a variety of metals, Ti, W, Pt, Co, Ni, Ta,

* Corresponding author, caross@mit.edu.
**Received for review: 07/6/2010**
**Published on Web: 08/10/2010**



DOI: 10.1021/nl1023518 | *Nano Lett.* **2010,** *10,* 3722–3726

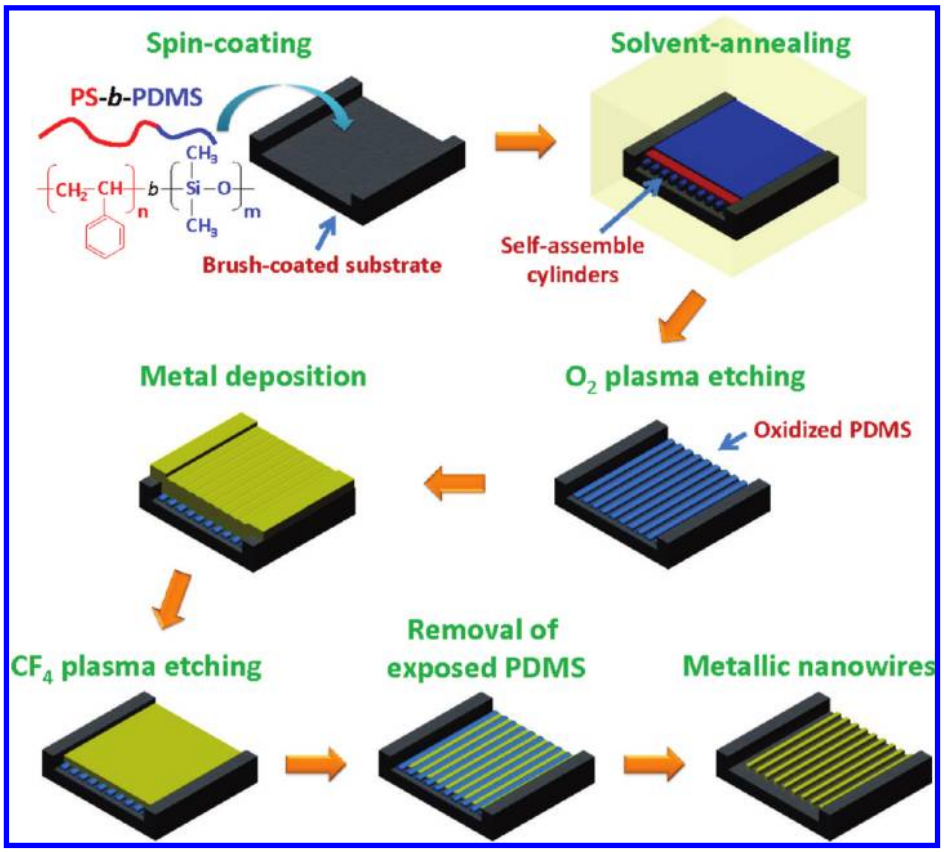


**FIGURE 1. The procedure for pattern formation by block copolymer self-assembly and pattern transfer using plasma etching.**

Au, and Al, to make nanowires of widths down to 9 nm that can be used as interconnect lines or memory device components, and we describe their magnetic and electrical properties. The process used here resembles a damascene pattern-transfer technique, which requires neither a specific etch-chemistry nor a sharp edge profile of the BCP pattern.

Figure 1 schematically illustrates the processes of BCP self-assembly and pattern transfer. The self-assembly process using PS-PDMS BCPs, including the critical role of brush treatment and solvent−vapor annealing conditions, were described in detail in our previous reports.[12−15] More recently, we also reported the extensive tunability of pattern dimension and geometry using mixed solvent vapors.[18] Figure 2 demonstrates the steps in the fabrication of W nanowires using BCP templates made from 45.5 kg/mol PS-PDMS. The block copolymer is solvent annealed to form a monolayer of in-plane cylinders of PDMS in a PS matrix with a PDMS surface layer. A two-step reactive ion etching process composed of short $CF_4$ and $O_2$ plasma treatments removes the surface layer and the PS matrix, leaving oxidized PDMS cylinders shown in panels a and b of Figure 2. The measured average period and line width are $33.8 \pm 0.41$ and $14.2 \pm 0.2$ nm, respectively. The self-assembly was uniform over a large scale substrate (area $\sim 5$ cm$^2$). A W film was then deposited on top of the oxidized PDMS grating pattern. From the images, it can be seen that the surface of the W film shows a small fluctuation in film topography but

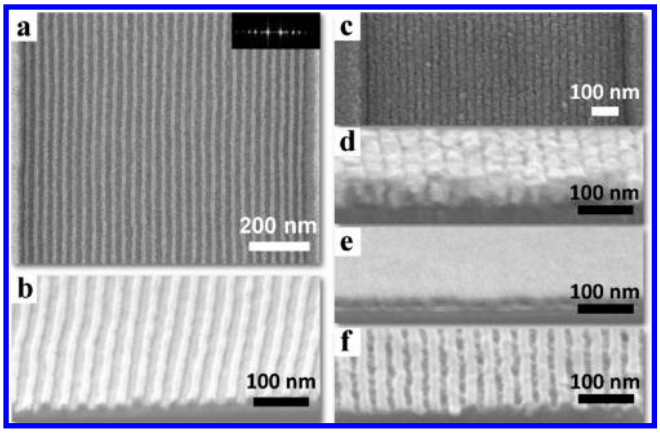


**FIGURE 2. An example of pattern transfer from self-assembled patterns into metal films, showing top view and tilted scanning electron microscopy (SEM) images at different stages of the process. (a, b) The oxidized PDMS pattern after self-assembly and reactive ion etching. (c, d) 55 nm thick W deposited on the oxidized PDMS pattern. (e) W surface after $CF_4$ plasma etching, showing smoothing. (f) W nanowires after the etch is complete.**

is smoother than the underlying PDMS patterns presented in panels a and b of Figure 2, illustrating partial planarization. The deposited film was etched back with a $CF_4$ plasma. Initially the metallic film was slowly sputter-etched by energetic $CF_x$ species, which planarizes the metal film since the peaks are etched faster than the valleys due to shadowing effects. This self-smoothing is an essential part of the



DOI: 10.1021/nl1023518 | *Nano Lett.* **2010,** *10,* 3722–3726

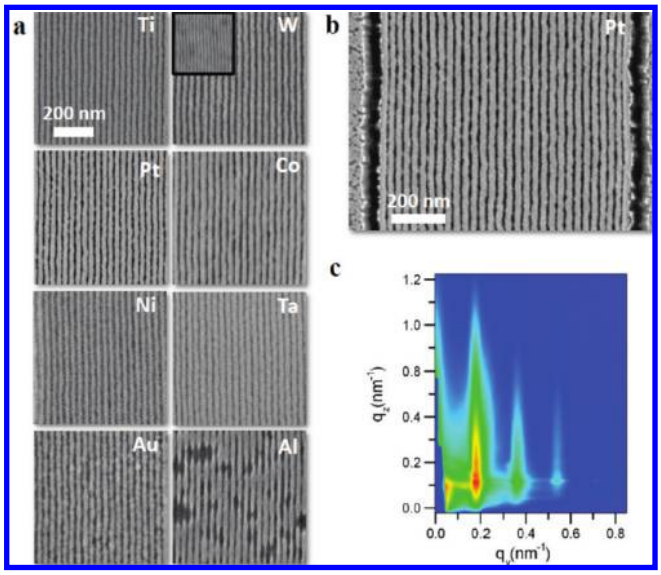


**FIGURE 3. (a)Various metallic (Ti, W, Pt, Co, Ni, Ta, Au, and Al) nanowires with 14−20 nm line width fabricated using the 45 kg/mol cylinder-forming PS-PDMS. The inset to the W image shows W wires of 9 nm width, 17 nm period formed using 16 kg/mol PS-PDMS at the same magnification. (b) A larger area view of the Pt nanowires also showing the wires adjacent to the step edges. (c) GISAXS pattern of the Pt nanowire sample showing several diffraction orders, indicative of good long-range orientational order and uniform periodicity.**

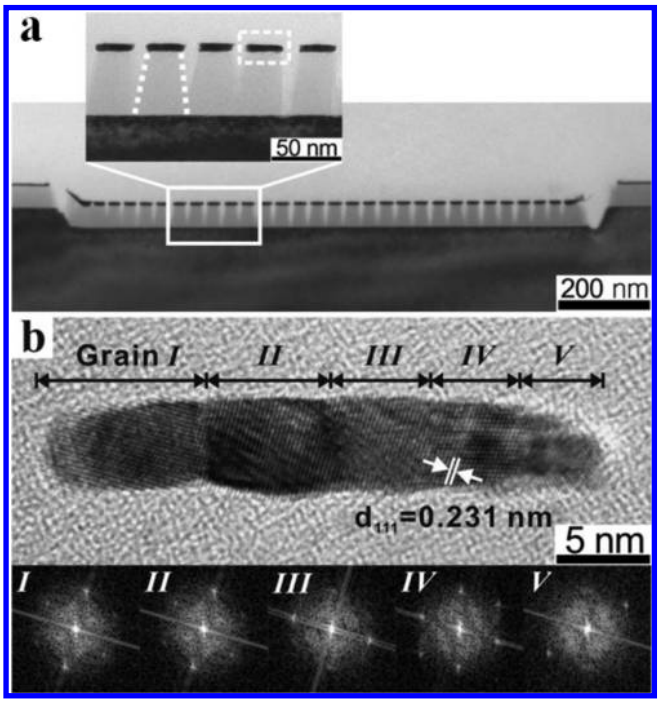


**FIGURE 4. (a) A low-magnification cross-sectional TEM image of Pt nanowires. (b) An enlarged high-resolution TEM image from the rectangular region marked with a dashed box in the inset of (a) and fast Fourier transformation images acquired from the five grains in the Pt nanowire cross section.**

image reversal process depicted in Figure 1. As soon as the buried PDMS pattern was exposed to the plasma, it was removed much faster than the metal. Terminating the etch process at that point results in a reverse-contrast image in the W film with a thickness equal to that of the BCP pattern. The etch rates of metallic films range from 2.3 to 25 nm/min compared to 140 nm/min for the oxidized PDMS,[17] and thus once the buried PDMS patterns are exposed to the 450 W $CF_4$ plasma, they are etched away in 6 s. The electrical resistance of the metallic films was monitored during the plasma etching process in order to estimate the remaining thickness and to prevent overetching.

Figure 3a demonstrates a range of metallic nanowire patterns with a pattern density of $2.94 \times 10^5$ cm$^{-1}$ made using 45.5 kg/mol PS-PDMS. This universal pattern-transfer technique was also successful with higher-density self-assembled patterns made with a 16 kg/mol PS-PDMS annealed in acetone,[19] yielding 9 nm wide W nanowires with 17.5 nm period, a pattern density of $5.71 \times 10^5$ cm$^{-1}$. These are shown as an inset to the W image, at the same magnification. Of the materials patterned, Au and Al gave poorer quality wires, which is attributed to surface diffusion induced by energetic ion bombardment. The outermost wires, formed adjacent to the trench edges were rougher and wider, as seen in Figure 3b and Figure 4a, due to the edge roughness of the trench. The long-range ordering and uniformity of the metallic nanostructures over the centimeter-scale substrate are confirmed by a grazing-incidence small-angle X-ray scattering (GISAXS) measurement on Pt wires (Figure 3c), which shows well-resolved diffraction patterns with high-order peaks.

This patterning process has several advantages over conventional dry etching methods using an etch-mask or lift-off techniques. In general, self-assembled polymer patterns are not sufficiently robust as an etch-mask for direct patterning of underlying metallic films, necessitating a stack of multilayer films for pattern transfer and multiple reactive ion etching and ion-milling processes.[20] Although a lift-off process can avoid these complexities, it suffers from other challenges due to the low aspect ratio of templates obtained from in-plane cylinders or spheres, and precludes the use of nondirectional deposition techniques such as sputtering or chemical vapor deposition methods. The successful fabrication of various metallic nanowires in this study confirms that the back-etch process described here can effectively mitigate these practical issues.

Figure 4a shows a low-magnification transmission electron microscopy (TEM) cross-section image of Pt nanowires aligned in a trench. The average cross-sectional area of the polycrystalline Pt nanowires excluding the wires directly adjacent to the step edges is highly uniform, 199.8 nm$^2$ ± 10.6 nm$^2$, and the height of the Pt nanowires is approximately 5 nm. This is smaller than the height (∼10−12 nm) of the self-assembled oxidized PDMS features, due to overetching of the metal. The underlying 20 nm thick $SiO_2$ film was also etched, and consequently V-shaped grooves were formed between adjacent Pt nanowires. On the basis



DOI: 10.1021/nl1023518 | *Nano Lett.* **2010,** *10,* 3722–3726

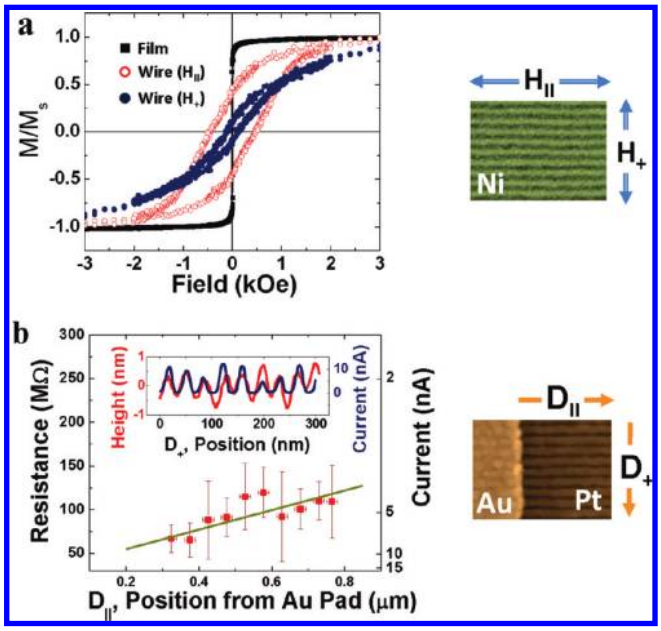


**FIGURE 5. Physical properties of fabricated nanowire patterns. (a) Magnetic hysteresis curves of an unpatterned Ni film and Ni nanowires. The magnetic field was applied parallel ($H_{II}$) or perpendicular ($H_+$) to the long axis of the nanowires as indicated in the SEM image. (b) Resistance of Pt nanowires measured with conductive atomic force microscopy (C-AFM). The C-AFM tip scanned the Pt nanowires near the Au pad, and current was recorded at varying distances from the Au contact pad parallel to the wires. The inset shows height and current profiles along a direction $D_+$ parallel to the edge of the pad.**

of the high-resolution TEM image and five fast Fourier transform images of each grain visible in the cross section (Figure 4b), the Pt nanowires are polycrystalline, with grain widths in the cross section of 4.4−9.1 nm. From the *d*-spacing (=0.231 nm) of the (111) planes, the lattice parameter is estimated to be 0.400 nm, which is similar to that of bulk Pt, 0.392 nm.[21] The stress perpendicular to the wires is likely to be largely relaxed, but there may still be stress along the wire length since sputter-deposited thin films are typically compressively stressed.[22]

Magnetic nanowires can potentially be used for high-density magnetic memory or logic devices based on domain wall motion.[23,24] Ni nanowires made in this study (Figure 5a) maintained their ferromagnetism after patterning and showed a strong in-plane anisotropy along the wire axis and a higher saturation field in plane, transverse to the wire axis as expected from the shape anisotropy.[25] The coercivity parallel ($H_{II}$) and transverse ($H_+$) to the wires was 470 and 119 Oe, respectively, compared to 17 Oe for an unpatterned Ni film of 12 nm thickness. The Supporting Information (Figure S3) shows micromagnetic simulation results for this wire geometry. The model predicts a lower coercivity for the field applied transverse to the wires, as seen experimentally. The experimental result in Figure 5a shows a lower loop squareness compared to the simulation result due to distribution in switching fields of the wires caused by edge roughness and other microstructural differences. These results indicate that the patterning yields separated wires (as seen for Pt by TEM) without degrading the magnetic properties of the Ni. The volume-averaged magnetic moment for the wires is 75% that of a continuous film, which most likely reflects oxidation of the Ni at the sidewalls of the wires or errors in film thickness estimation.

The resistance of metallic nanowires is of interest for interconnects, and as an example the electrical conductivity of the Pt nanowires (Figure 5b) was characterized using conductive atomic force microscopy. A 50 nm thick gold pad was evaporated on the Pt nanowires and grounded during the measurement, and the average current flowing through a group of 10 Pt nanowires was measured as a function of distance from the Au pad. The inset to Figure 5b demonstrates a good matching in periodicity between the topography and current profiles, on scanning transverse to the wires. Due to the larger tip radius (∼20 nm) compared to the spacing (∼13 nm) between two Pt nanowires, the peak−valley height variation is much smaller than the physical depth (∼30 nm). The average current decreased monotonically with distance, which implies that the resistance of the nanowires scales linearly with the nanowire length, and the resistivity of the Pt nanowires was around 2.19 $\Omega \cdot$cm. This resistivity is orders-of-magnitude larger than that (=10.6 $\mu\Omega \cdot$cm) of bulk Pt, probably due to enhanced scattering from the grain boundaries in the fine-grained film and from the surfaces of the wires.

In summary, we have demonstrated the formation of aligned metallic wire patterns or gratings with excellent long-range order on substrate patterned with a micrometer-scale guiding template. The fabrication process relies on block copolymer self-assembly combined with a versatile pattern-transfer technique. Electrical measurements indicate continuity of the nanowires, while magnetic measurements are consistent with an array of magnetically isolated structures. The structural arrangement and the magnetic and electrical properties of the nanowire arrays suggest that this technique will be effective for the realization of highly integrated nanoscale electrical and magnetic devices, especially when combined with methods to generate more complex structures such as lines with bends or junctions.[26] In addition, metal nanowires can potentially be used as catalysts for making carbon nanostructures, as gratings in optical polarizers,[27−29] or for studies of dewetting phenomena or Rayleigh instabilities in confined geometries.

**Experimental Section.** A cylinder-forming PS-PDMS block copolymer (Polymer Source, Inc.) with total molecular weight of 45.5 kg/mol and nominal volume fraction of PDMS, $f_{DMS}$ = 33.5% was used for most experiments. Substrates patterned with 40 nm deep trenches with a periodicity of 1.3 $\mu$m were fabricated using a Lloyd's Mirror interference lithography system with a 325 nm wavelength He−Cd laser. The laser exposed grating patterns into a 200 nm thick PFI-88 photoresist (Sumitomo Chemical Co.), which were transferred into the Si substrate by a 10 mTorr $CF_4$ reactive ion



DOI: 10.1021/nl1023518 | *Nano Lett.* **2010,** *10,* 3722–3726

etching. The native oxide surfaces were treated by hydroxy-terminated PDMS homopolymer with molecular weight 5 kg/mol, which was spun-cast on the substrates and annealed at 150 °C for 15 h, then washed with toluene to remove unattached polymers. The thickness of the grafted brush layer was estimated to be around 3−4 nm by ellipsometry. BCP thin films with a thickness of 30 nm were obtained by spin-casting toluene solutions of 1.5% by weight of the block copolymer on the substrates, then the samples were solvent-annealed under toluene or toluene/heptane vapor at room temperature for 3 h. The annealed film was treated with a 5 s, 50 W $CF_4$ plasma followed by a 22 s, 90 W $O_2$ plasma to remove the PDMS surface layer and selectively eliminate the PS block, resulting in oxidized PDMS microdomains in the trenches. A 16 kg/mol PS-PDMS was also used in some experiments and was solvent annealed in a low vapor pressure of acetone.[19] Metallic thin films of Ti, W, Co, Ta, Ni, and Pt with a thickness of 55−70 nm were deposited using an rf sputtering system (base pressure = $1 \times 10^{-8}$ Torr, working pressure = 2 mTorr, and power = 300 W) on top of the block copolymer patterns and etched with a 450 W, 10 mTorr $CF_4$ plasma for 2−25 min depending on the etch rate and film thickness. At first the metal was physically removed by ionized $CF_x$ species, but after the buried block copolymer patterns (or underlying silica substrate) were exposed to the plasma, they formed volatile $SiF_x$ and were etched quickly.[16] As a result, arrays of metallic nanowires were obtained. The surface morphology was observed using a Zeiss/Leo Gemini 982 scanning electron microscope operated with an acceleration voltage of 5 kV. A thin layer of Au−Pd alloy was sputter-coated on the samples in order to avoid charging effects. The microstructural characterization was performed by TEM (in a JEOL JEM-3010). The cross-sectional TEM sample was mechanically polished and ion-milled at low current $Ar^+$ ion dose to minimize damage. GISAXS experiments were performed at the G1 beamline at the Cornell High Energy Synchrotron Source (CHESS). The wavelength of the incident beam was 1.239 Å, with a sample to detector distance of 1122 mm and an incidence angle of 0.1°. A slow-scan CCD-based X-ray detector was used for data collection.

**Acknowledgment.** The authors thank the Semiconductor Research Corporation, the Office of Naval Research, the National Research Foundation Grant (KRF-2008-314-D00153), and the BK21 program for financial support and Dr. Eric Verploeggen for GISAXS measurements.

**Supporting Information Available.** Figures showing polymer patterning, an example of pattern transfer, micromagnetic simulation results of ferromagnetic Ni nanowires as a function of field direction and number of wires, and C-AFM measurement results of Pt nanowires. This material is available free of charge via the Internet at http://pubs.acs.org.

## REFERENCES AND NOTES

(1) Cui, Y.; Lieber, C. M. *Science* **2001**, *291*, 851–853.
(2) Huang, Y.; Duan, X. F.; Cui, Y.; Lauhon, L. J.; Kim, K. H.; Lieber, C. M. *Science* **2001**, *294*, 1313–1317.
(3) Cui, Y.; Wei, Q. Q.; Park, H. K.; Lieber, C. M. *Science* **2001**, *293*, 1289–1292.
(4) Chai, J.; Wang, D.; Fan, X. N.; Buriak, J. M. *Nat. Nanotechnol.* **2007**, *2*, 500–506.
(5) Law, M.; Goldberger, J.; Yang, P. D. *Annu. Rev. Mater. Res.* **2004**, *34*, 83–122.
(6) Duan, X. F.; Huang, Y.; Cui, Y.; Wang, J. F.; Lieber, C. M. *Nature* **2001**, *409*, 66–69.
(7) Huang, Y.; Duan, X. F.; Wei, Q. Q.; Lieber, C. M. *Science* **2001**, *291*, 630–633.
(8) Leibler, L. *Macromolecules* **1980**, *13*, 1602–1617.
(9) Cheng, J. Y.; Ross, C. A.; Chan, V. Z. H.; Thomas, E. L.; Lammertink, R. G. H.; Vancso, G. J. *Adv. Mater.* **2001**, *13*, 1174–1178.
(10) Milliron, D. J.; Raoux, S.; Shelby, R.; Jordan-Sweet, J. *Nat. Mater.* **2007**, *6*, 352–356.
(11) Black, C. T. *Appl. Phys. Lett.* **2005**, 87.
(12) Jung, Y. S.; Ross, C. A. *Nano Lett.* **2007**, *7*, 2046–2050.
(13) Bita, I.; Yang, J. K. W.; Jung, Y. S.; Ross, C. A.; Thomas, E. L.; Berggren, K. K. *Science* **2008**, *321*, 939–943.
(14) Jung, Y. S.; Jung, W.; Ross, C. A. *Nano Lett.* **2008**, *8*, 2975–2981.
(15) Jung, Y. S.; Jung, W.; Tuller, H. L.; Ross, C. A. *Nano Lett.* **2008**, *8*, 3776–3780.
(16) Jung, Y. S.; Jung, W.; Ross, C. A. *Nano Lett.* **2008**, *8*, 2975–2981.
(17) Jung, Y. S.; Ross, C. A. *Small* **2009**, *5*, 1654–1659.
(18) Jung, Y. S.; Ross, C. A. *Adv. Mater.* **2009**, *21*, 2540–2545.
(19) Jung, Y. S.; Chang, J. B.; Verploegen, E.; Berggren, K. K.; Ross, C. A. *Nano Lett.* **2010**, *10*, 1000–1005.
(20) Cheng, J. Y.; Ross, C. A.; Chan, V. Z. H.; Thomas, E. L.; Lammertink, R. G. H.; Vancso, G. J. *Adv. Mater.* **2001**, *13*, 1174–1178.
(21) *CRC Handbook of Chemistry and Physics*, 88th ed. (Internet Version 2008); Lide, D. R., Ed.; CRC Press/Taylor and Francis: Boca Raton, FL, 2008.
(22) Hoffman, D. W.; Thornton, J. A. *J. Vac. Sci. Technol.* **1982**, *20*, 355–358.
(23) Hayashi, M.; Thomas, L.; Moriya, R.; Rettner, C.; Parkin, S. S. P. *Science* **2008**, *320*, 209–211.
(24) Parkin, S. S. P.; Hayashi, M.; Thomas, L. *Science* **2008**, *320*, 190–194.
(25) Garcia, J. M.; Asenjo, A.; Velazquez, J.; Garcia, D.; Vazquez, M.; Aranda, P.; Ruiz-Hitzky, E. *J. Appl. Phys.* **1999**, *85*, 5480–5482.
(26) Yang, J. K. W.; Jung, Y. S.; Chang, J. B.; Mickiewicz, R. A.; Alexander-Katz, A.; Ross, C. A.; Berggren, K. K. *Nat. Nanotechnol.* *5*, 256–260.
(27) Schider, G.; Krenn, J. R.; Gotschy, W.; Lamprecht, B.; Ditlbacher, H.; Leitner, A.; Aussenegg, F. R. *J. Appl. Phys.* **2001**, *90*, 3825–3830.
(28) Wang, J. J.; Deng, J. D.; Deng, X. G.; Liu, F.; Sciortino, P.; Chen, L.; Nikolov, A.; Graham, A. *IEEE J. Sel. Top. Quantum Electron.* **2005**, *11*, 241–253.
(29) Wang, J. J.; Zhang, W.; Deng, X. G.; Deng, J. D.; Liu, F.; Sciortino, P.; Chen, L. *Opt. Lett.* **2005**, *30*, 195–197.



DOI: 10.1021/nl1023518 | *Nano Lett.* **2010,** *10,* 3722–3726